CHEMISTRY OF MATERIALS

Article

pubs.acs.org/cm

Mechanism of Zn Particle Oxidation by H_2O and CO_2 in the Presence of ZnO

David Weibel,[†] Zoran R. Jovanovic,*[,†] Elena Gálvez,[†] and Aldo Steinfeld[†,‡]

[†]Department of Mechanical and Process Engineering, ETH Zurich, Zurich 8092, Switzerland

[‡]Solar Technology Laboratory, Paul Scherrer Institute, Villigen 5232, Switzerland

Supporting Information

ABSTRACT: In this work we investigate the mechanism of Zn oxidation with CO_2 and/or H_2O to produce solar derived fuels (CO and/or H_2) as part of the Zn/ZnO thermochemical redox cycle. It has been observed that the ZnO contamination of Zn produced by solar thermal reduction of ZnO (solar Zn) facilitates oxidation of the metallic Zn by CO_2 and H_2O, allowing for nearly complete conversion at temperatures as low as 350 °C. Reaching the same reaction extent starting with pure Zn requires considerably higher temperatures which imposes use of unconventional hard-to-operate reaction configurations utilizing Zn as vapor. The mechanism of this enhancement is investigated by studying the oxidation of solid Zn diluted with ZnO or Al_2O_3 at 350−400 °C utilizing thermogravimetry. It is found that ZnO acts as the site for the oxidation of Zn originating from the vapor phase, thereby serving as a sink for Zn vapor and maintaining the driving force for sustainable Zn sublimation. As this Zn sublimation competes with the growth of an impervious ZnO scale over the surface of the remaining solid Zn, the presence of the ZnO increases the reaction extent according to the magnitude of its surface area. This mechanism is supported by energy-dispersive X-ray (EDX) spectroscopy, revealing a substantial deposition of produced ZnO over the surface of the ZnO-seeded Al_2O_3 diluent.

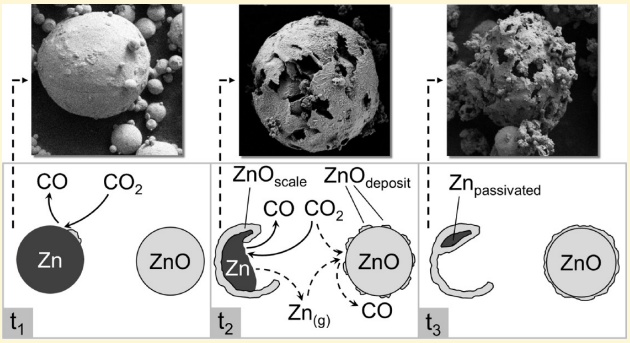

1. INTRODUCTION

Because of the high O_2-looping capacity per unit mass of Zn, the thermochemical Zn/ZnO redox cycle has been considered as an attractive path toward producing solar fuels.[1,2] In the first step that takes place at temperatures in the vicinity of 1800 °C (eq 1), ZnO is thermally reduced into a gaseous mixture of Zn and O_2 using concentrated solar radiation as the heat source. Upon quenching by inert gas, this mixture yields a powder consisting of Zn and ZnO also known as "solar Zn".[3] In the following step performed at temperatures in the range 350−1000 °C (eq 2), the solar Zn is oxidized by H_2O and/or CO_2 to produce fuel (H_2 and/or CO) and ZnO which is then fed into the reduction step to close the cycle.[4,1]

$$\mathrm{ZnO} \rightarrow \mathrm{Zn} + 0.5\mathrm{O_2}$$
$$\Delta h^\circ = 350.5\ \mathrm{kJ/mol} \quad (1)$$

$$\mathrm{Zn} + x\mathrm{CO_2} + (1-x)\mathrm{H_2O} \rightarrow \mathrm{ZnO} + x\mathrm{CO} + (1-x)\mathrm{H_2}$$
$$\Delta h^\circ = -108.8 + 41.3x\ \mathrm{kJ/mol} \quad (2)$$

The overall cycle efficiency is measured by the heating value of the fuel produced per total energy input. Thermodynamic calculations have shown that it increases with an increase in the yield of fuel (H_2 and/or CO), thus the extent of both reactions 1 and 2.[5] However, it has also been shown that achieving a high extent of reaction 1 requires ultrafast quenching of the product mixture to suppress the recombination of Zn-vapor and O_2.[1] This task is generally performed by mixing substantial amounts of inert gas with the solar reactor product stream,[6] which adversely affects the cycle efficiency due to the additional energy required for purification and recycling of the inert gas quencher. Nevertheless, the solid product leaving the quencher as "solar Zn" generally contains substantial amount of ZnO.[6,7]

At the same time, the studies of reaction 2 have shown that below its melting temperature (420 °C) the pure metallic Zn reacts rather slowly with either CO_2[8,9] or H_2O.[10−12] Moreover, the complete oxidation is not possible due to the passivation of the Zn surface by the impervious ZnO product scale.[8,13] For this reason, previous investigators have proposed the use of Zn as either liquid[14] or aerosol nanoparticles/droplets precipitated from *in situ* quenched Zn-vapor[5,15−20] as the preferred paths toward a high extent of the oxidation. These, however, not only impose unconventional, hard-to-operate oxidizer reactor concepts but they also require the additional energy to melt and/or vaporize Zn that has an adverse impact on the overall cycle efficiency.

Received: August 20, 2014
Revised: October 20, 2014
Published: October 23, 2014

   dx.doi.org/10.1021/cm503064f | Chem. Mater. 2014, 26, 6486−6495

Recent research has demonstrated that the ZnO contamination of Zn produced by solar thermal reduction of ZnO in fact facilitates the oxidation of the metallic Zn with either CO_2 or H_2O.[21,22] It has been shown that the oxidation of solar Zn by CO_2 could be almost completed at temperatures as low as 350 °C in the matter of minutes (~90% conversion in 180 s).[22] This reaction time is indeed 2-orders of magnitude longer than the residence time reported for the equivalent conversion of Zn vapor (~1 s).[20] However, becaue of the difference between the feedstock densities (~0.7 kg/m^3 for Zn-vapor at 1000 °C versus ~440 kg/m^3 for solar Zn containing only 25 wt % Zn[23]) the reactor volumes required for oxidizing solar Zn and Zn-vapor at the equivalent fuel productivity are about the same.

Proper choice and design of a solar Zn oxidizer reactor should be guided by a reliable kinetic model that is based on a plausible reaction mechanism. In particular, such a mechanism must be able to account for the pivotal role of ZnO in enhancing Zn oxidation. This enhancement has been recently attributed to a rather general multireaction scheme postulated by Stamatiou et al.[22] The objective of this work is to further refine this scheme and discriminate pertinent reaction pathways. For this purpose the oxidation of solar Zn was simulated by the oxidation of Zn in blends with ZnO or Al_2O_3 diluents prepared from well characterized commercial powders. The oxidation of diluted Zn particles was explored by thermogravimetry as a function of the specific area and chemical nature of the diluent surface. The refined oxidation mechanism was supported by the evidence provided by transmission electron microscopy (TEM), scanning TEM (STEM), and electron dispersive X-ray spectrometry (EDX).

2. EXPERIMENTAL SECTION

2.1. Materials and Methods. The solar Zn surrogates were prepared by blending commercially available Zn (Sigma-Aldrich, >98% purity) and ZnO powders (Strem Chemicals or Grillo). In some experiments, Al_2O_3 powder (Strem Chemicals) was used as an alternative to ZnO to assess the specific role of the chemical nature of the diluent surface. To further investigate the effect of the diluent surface, some blends were prepared from ingredients that were immersed in water or ethanol and then dried at room temperature. These materials are referred in further text as water- or ethanol-pretreated. All blends were prepared by shaking equivalent 8−9 mg aliquots of the Zn and a diluent in a covered Petri dish for 3 min with occasional stirring and breaking agglomerates with a spatula. No segregation of the ingredients was observed.

The raw materials were analyzed for particle size distribution (HORIBA LA-950 laser scattering analyzer), Brunauer−Emmett−Teller (BET) equivalent specific surface area (Micrometrics TriStar 3000 N_2 absorption analyzer) and particle morphology (scanning electron microscopy (SEM), Zeiss Supra 55VP and Hitachi TM-1000). The volume-based mean particle sizes $\bar{d}$ and the BET-equivalent surface areas of the materials are listed in Table 1. Figure 1 indicates broad size distributions of Al_2O_3 and ZnO (Strem) particles and narrower, rather similar distributions of the Zn and ZnO (Grillo) particles. The SEM pictures of ZnO (Strem) (Figure 2c,d) and Al_2O_3 powders (Figure 2e,f) reveal the origin of their large BET areas in spite of the relatively large mean particle sizes: both materials comprised porous micron-sized agglomerates of finer nanosized grains. The Al_2O_3 BET area is additionally enlarged by a porous structure of the grains (average pore diameter of 2.8 nm as reported by the manufacturer). The BET areas of the round, smooth Zn particles (Figure 3) and the needle-like ZnO (Grillo) agglomerates (Figure 2a,b) were about 2 orders of magnitude smaller. Reacted samples were examined by TEM, STEM, and EDX performed with a FEI Tecnai F30ST instrument. The TEM sample was prepared by dispersing the investigated particles on a carbon-sputtered Cu mesh holder.

Table 1. Properties of the Powder Reactants

material	$\bar{d}$ (μm)	BET (m^2/g)
ZnO Strem	33.9	95[a]
ZnO Grillo	6.5	2.9
Al_2O_3	4.9	305[a]
Zn	6.7	1.5

[a]As reported by the manufacturer.

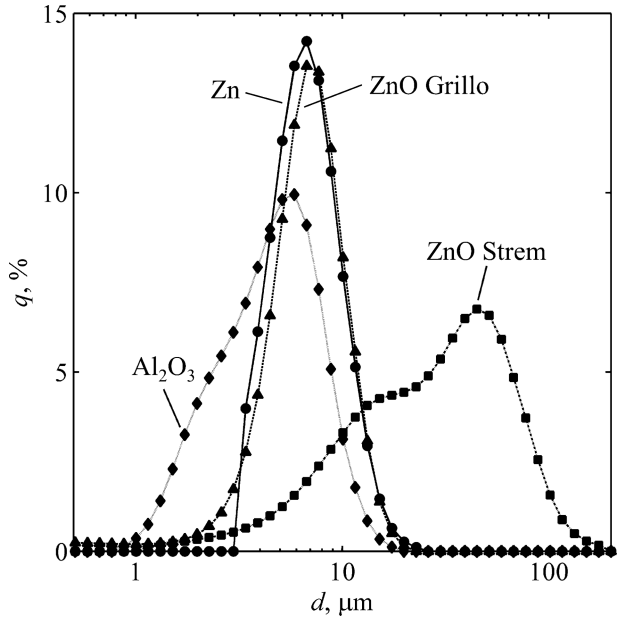

Figure 1. Volume-based particle size distributions of the used Zn, ZnO, and Al_2O_3 powders.

2.2. TG Analysis. Oxidation of solar Zn surrogate blends was studied isothermally in a thermogravimetric analyzer (Netzsch 409 STA) at temperatures between 350 and 400 °C (below the melting point of Zn). Gas mixtures of Ar (Messer 5.0) with CO_2 (Messer 4.8) or H_2O (generated by aDROP DV2 steam generator) served as the reacting gases. The composition of the product gas was analyzed by a gas chromatograph (GC Varian cp4900 with Molsieve-5A/Poraplot-U columns). The TG setup has been attested for measuring the kinetics free of mass and heat transfer intrusion as described elsewhere.[22]

A cylindrical alumina crucible containing the sample was positioned on an alumina shielded S-type thermocouple inside the TG furnace and heated in Ar to a designated oxidation temperature at a rate of 10 K/min. After the sample temperature reached steady-state, the oxidizing gas flow was started at the balance reading designated as the initial sample mass m_0. Once asymptotic conversion was attained under isothermal conditions, the sample was heated up to 800 °C at 10 K/min in 15% CO_2−Ar and kept at this temperature until all the remaining Zn was oxidized as reflected by a constant final sample mass m_f.

The total mass of Zn available for the oxidation ($m_{Zn,tot}$) and temporal Zn conversion (X) were calculated as

$$m_{Zn,tot} = \frac{m_f - m_0}{M_O} M_{Zn} \quad (3)$$

and

$$X(t) = \frac{m(t) - m_0}{m_f - m_0} \quad (4)$$

where M_i and $m(t)$ designate molecular mass of species i and temporal sample mass, respectively. This method for determining $m_{Zn,tot}$ and X eliminates errors potentially brought in by the loss of Zn during

dx.doi.org/10.1021/cm503064f | Chem. Mater. 2014, 26, 6486−6495

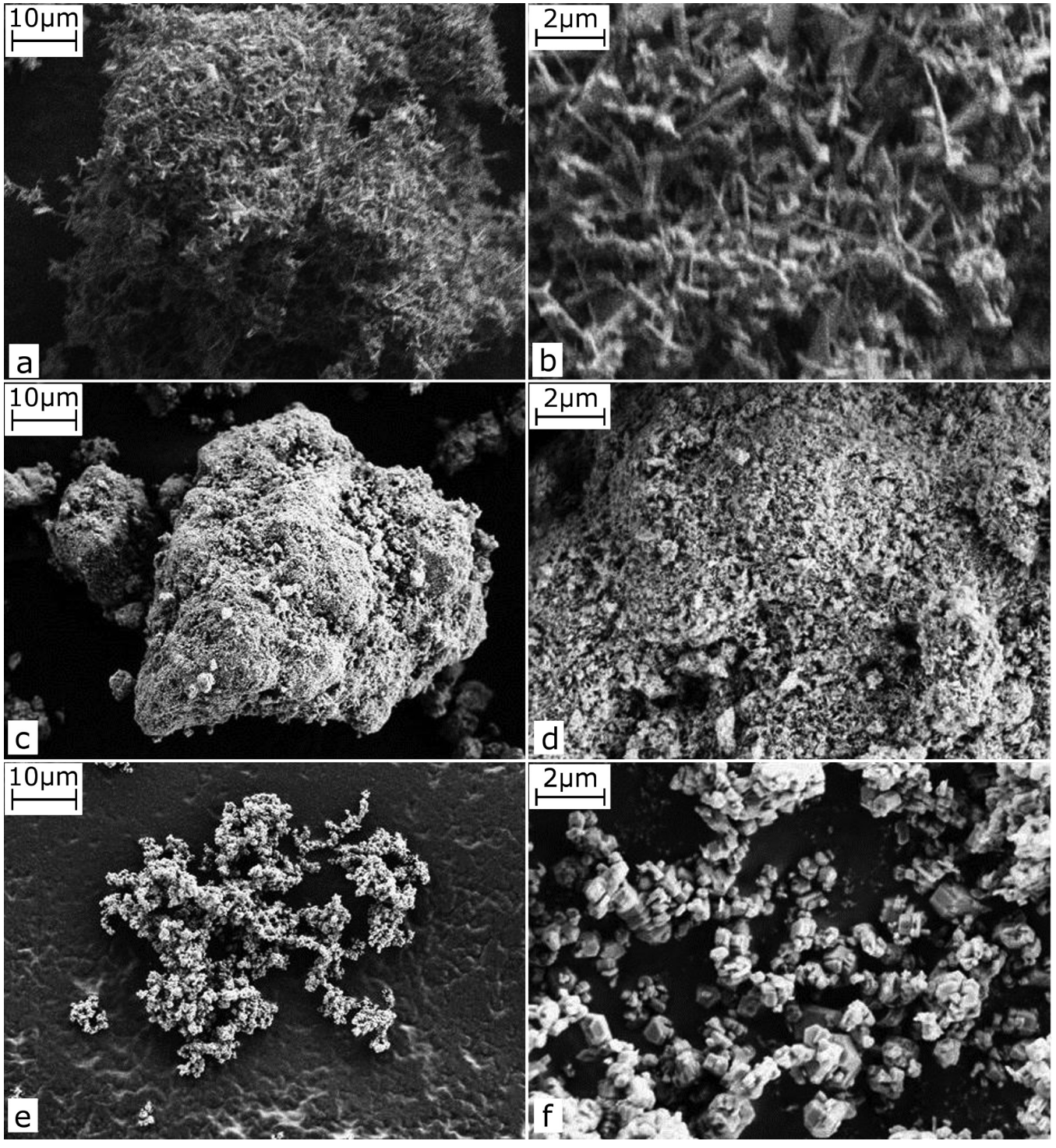

Figure 2. SEM images of the materials used as Zn diluents: ZnO (Grillo) (a, b), ZnO (Strem) (c, d), and Al_2O_3 (Strem) (e, f).

sample handling and desorption of impurities during the heat-up to the reaction temperature. The implementation of the method was reflected by remarkable repeatability of the results and good agreement with previous work.[22]

3. RESULTS AND DISCUSSION

3.1. Effect of the ZnO Diluent on Zn Oxidation with CO_2. The work by Stamatiou et al.[22] has reported the facilitating effect of ZnO diluents on the Zn oxidation with CO_2 as a function of the mass fraction of different ZnO sources that, however, had similar specific surface areas and mean particle sizes. As the mass fraction of a ZnO diluent in a homogeneous blend with Zn powder (w_{ZnO}) increases so do both the surface area of the ZnO per amount of Zn and the degree of the dispersion of the Zn particles. Therefore, the reported facilitating effect of an increase in w_{ZnO} on both oxidation rate and asymptotic conversion of Zn[22] could be attributed to either a more pronounced reaction path taking place on the ZnO surface or suppressed sintering of the Zn particles. In order to distinguish between these two effects, the previously reported CO_2 oxidation kinetics obtained with ZnO

dx.doi.org/10.1021/cm503064f | Chem. Mater. 2014, 26, 6486−6495

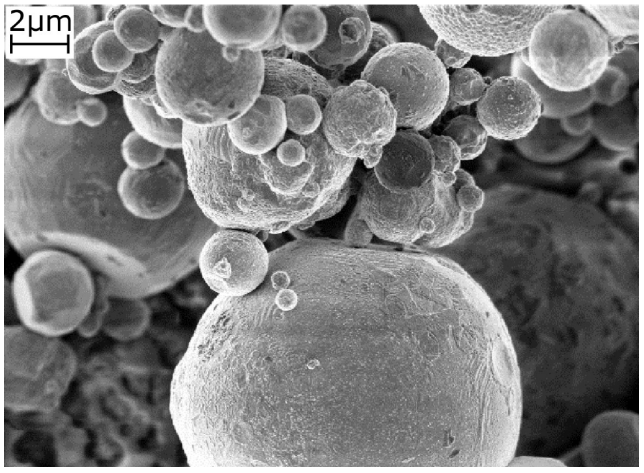

Figure 3. SEM image of the Zn particles used in the experiments.

(Grillo) diluent particles ($\bar{d}$ = 6.5 μm, SSA = 2.9 m^2/g)[22] was compared to the oxidation kinetics of Zn blended with larger but higher SSA ZnO (Strem) particles ($\bar{d}$ = 33.9 μm, SSA = 95 m^2/g) at the same w_{ZnO} = 0.5. The results shown in Figure 4 indicate that at the same reaction conditions (375 °C, 15% CO_2–Ar) Zn-ZnO (Strem) blends attained almost complete Zn conversion after 10 min, whereas Zn in a blend with ZnO (Grillo) reached the asymptotic conversion of only ~0.9 after 25 min. Moreover, at 350 °C the Zn-ZnO (Strem) blend performed similarly to the Zn-ZnO (Grillo) blend but at the temperature 25 °C higher, demonstrating also remarkable repeatability not attainable at such a low temperature with the Zn-ZnO (Grillo) blend.[22] As smaller ZnO (Grillo) particles should favor better dispersion of the Zn particles, the improvements brought in by larger but higher SSA ZnO (Strem) particles imply that higher Zn oxidation rates and asymptotic conversions both stem from the direct involvement of the ZnO surface in a reaction path parallel to the one leading to the passivation of the Zn surface.

3.2. Effect of the ZnO Diluent on Zn Oxidation with H_2O. When using H_2O as an oxidant instead of CO_2, the repeatability of experiments was poor. Additionally, overall conversion leveled off at lower values. This can be seen in Figure 5 showing Zn conversion curves for three repeated reactions of a 50 wt % Zn-ZnO (Grillo) blend in 8% H_2O–Ar at 400 °C. The repeatability of the results could not be improved by switching the ZnO source from Grillo to Strem or changing reaction conditions (sample mass, H_2O concentration, temperature). In contrast to the homogeneous appearance of products obtained by oxidation with CO_2, the samples reacted with H_2O exhibited a compacted brittle white/yellow top crust covering the gray remainder of the material underneath. As indicated by the SEM pictures of a 50 wt % Zn-ZnO (Strem) sample reacted at 400 °C in 8% H_2O–Ar shown in Figure S1 in the Supporting Information, the top crust (Figure S1a in the Supporting Information) consisted of larger agglomerates and the hollow shells that are typical for reacted Zn particles[8] while the powder collected from the bottom of the crucible (Figure S1b in the Supporting Information) consisted of smaller particles and spherical Zn particles that appeared barely reacted.

In order to investigate if the Zn remaining in the bottom layer of the samples that had been exposed to steam was passivated, a reacted 50 wt % Zn-ZnO (Strem) sample that had

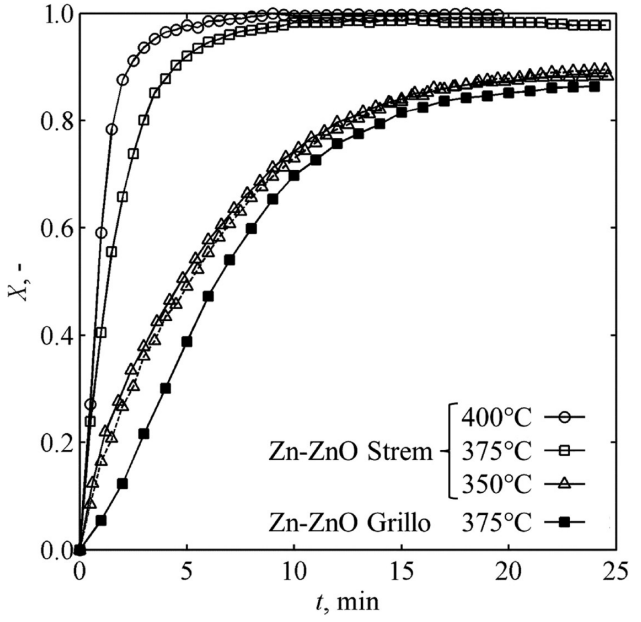

Figure 4. Zn conversion during reaction in 15% CO_2–Ar of 50 wt % Zn-ZnO blends prepared with ZnO (Strem) (open symbols) and ZnO (Grillo)[22] (filled squares). The dashed line designates a repeated experiment.

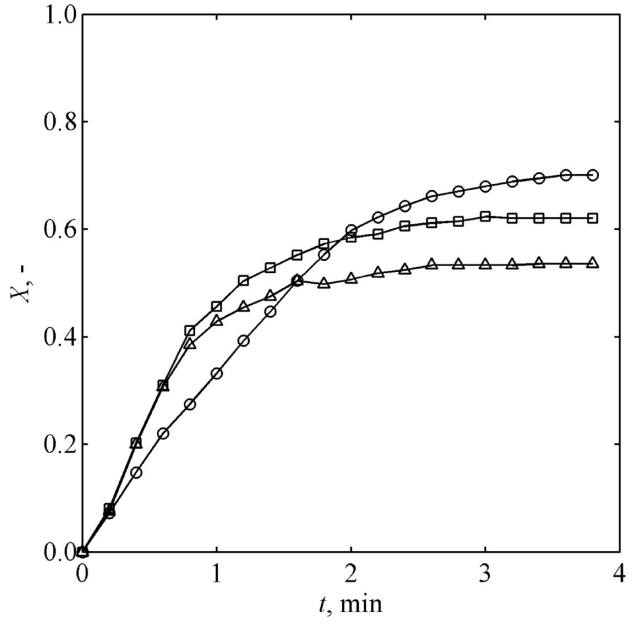

Figure 5. Zn conversion during reaction of a 50 wt % Zn-ZnO (Grillo) blend in 8% H_2O–Ar at 400 °C.

reached asymptotic conversion of ~0.3 at 375 °C in 30% H_2O–Ar was homogenized with a spatula and subjected again to the same conditions. The second run demonstrated additional conversion of ~0.05 calculated based on the Zn content at the beginning of the first run (Figure S2 in the Supporting Information). Conversely, Zn that reached asymptotic conversion in CO_2–Ar atmospheres could further react only when heated above 400 °C.[22] The limited Zn conversion in H_2O atmospheres is thus attributed to the top crust formed during the experiments that restricted the access of H_2O to the Zn in the bottom layer of the sample. The crust was likely formed by sintering of Zn and/or ZnO particles

dx.doi.org/10.1021/cm503064f | Chem. Mater. 2014, 26, 6486–6495

induced by the presence of H_2O in the atmosphere.[24] A similar problem has been encountered while carrying the same reaction in a packed bed reactor.[23] However, the TG oxidation of a real solar Zn in a H_2O atmosphere demonstrated the complete conversion of Zn[21] indicating that the sintering of the material may be specific to the investigated Zn-ZnO blends.

Although scrutinizing the ZnO diluent effect on the Zn oxidation with H_2O was precluded by a poor repeatability of the results, the Zn asymptotic conversions of 0.5−0.7 obtained with Zn-ZnO (Grillo) at 400 °C in 8% H_2O−Ar (Figure 5) are considerably higher than those reported for pure Zn having a similar particle size and reacting at the same temperature.[11,25] Therefore, the well documented favorable effect of the ZnO diluent on the Zn oxidation with CO_2 pertains to reactions with H_2O as well. It is therefore reasonable to assume that both oxidation reactions follow similar mechanisms involving the ZnO surface.

3.3. Effect of the Chemical Nature of the Diluent Surface. The next step in elucidating the mechanism of Zn oxidation in the presence of a diluent was to identify the type of reactions occurring on the diluent surface. The effect of the diluent surface chemistry was therefore examined by switching diluent from ZnO to Al_2O_3 as well as by surface modifications of the ingredients in Zn-diluent blends by ethanol- or water-pretreatment.

The temporal conversions of Zn blended with Al_2O_3 or ZnO (Strem) are compared in Figure 6 for oxidations with CO_2 or H_2O at 375 °C. In contrast to the Zn blended with ZnO, the Zn blended with Al_2O_3 exhibited no measurable conversion in CO_2. This finding is in agreement with previously reported results obtained with larger, segregating Al_2O_3 diluent particles ($\bar{d}$ = 81 μm).[22] At the same time, however, the Al_2O_3 diluent facilitates the oxidation of Zn with H_2O performing similarly to ZnO.

The diluent effect shown in Figure 6 implies that the ZnO diluent facilitates Zn oxidation with either H_2O or CO_2 while the Al_2O_3 contributes to the reaction only in the presence of H_2O. To clarify the origin of this difference, the effects of the diluent surface modifications was explored through the influence of powder pretreatments on the Zn oxidation with CO_2. Figure 7 compares the oxidation performance of a standard 50 wt % Zn-ZnO (Strem) blend in 15% CO_2−Ar at 375 °C with the performance of the same composition blends prepared with ZnO (Strem) powders that were prior to reaction subjected to water-wash, ethanol-wash, or a 4 h drying step at 450 °C under Ar flow. As seen in this figure, almost complete conversion could be attained with all these blends. Compared to the standard blend, ethanol-pretreated ZnO contributed to a slightly faster oxidation rate; the water-pretreated ZnO demonstrated the fastest decay in the oxidation rate underperforming even the dried out ZnO at Zn conversions greater than ∼0.4.Conversely, as illustrated in Figure 8 the performance of Zn−Al_2O_3 blends was substantially affected by either water- or ethanol-pretreatment of Al_2O_3 contributing to the asymptotic conversions as high as ∼0.9 and 0.75, respectively. As the Zn particles pretreated with ethanol, dried at room temperature, and then blended with the standard Al_2O_3 powder did not show any reactivity under the same reaction conditions (run not shown), the enhancements by the water- and ethanol-pretreatments demonstrated in Figure 8 have been attributed solely to the surface modifications of Al_2O_3.

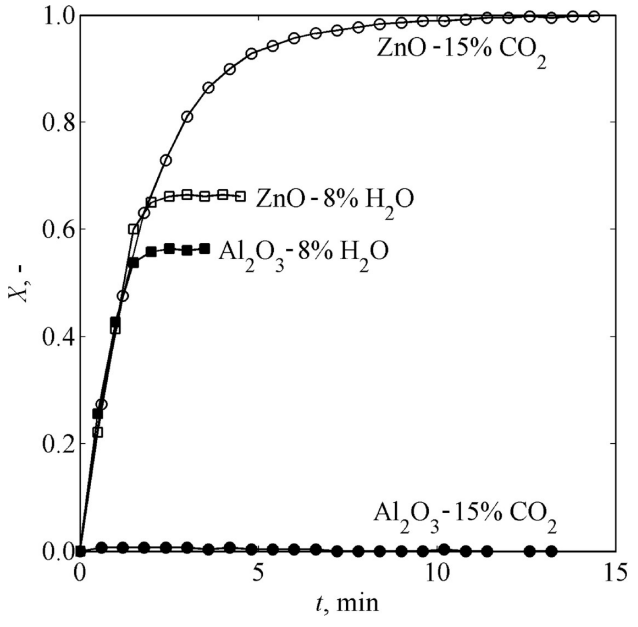

Figure 6. ZnO (Strem) versus Al_2O_3 (Strem) diluent effect on Zn oxidation with CO_2 or H_2O at 375 °C.

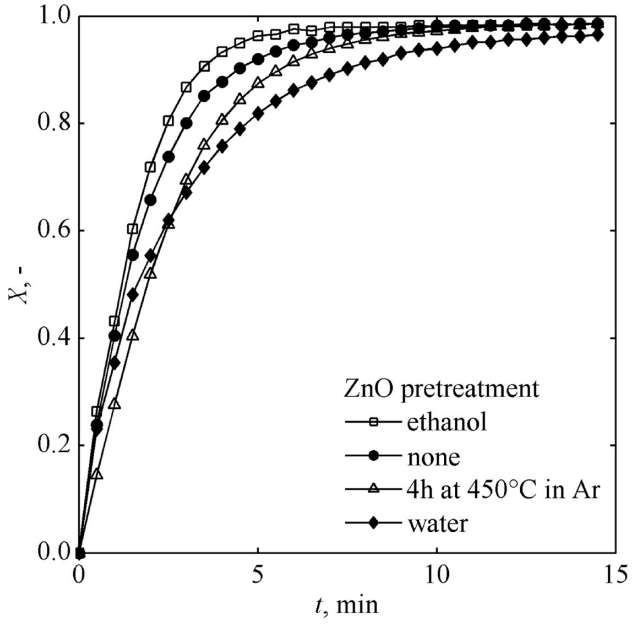

Figure 7. Effect of ZnO (Strem) pretreatment on the Zn conversion during reaction of 50 wt % Zn-ZnO blends at 375 °C in 15% CO_2−Ar.

3.4. Activation of the Al_2O_3 Diluent for Zn Oxidation with CO_2. Understanding why untreated Al_2O_3 does not promote Zn oxidation with CO_2 and how it is activated by the ethanol- or water-pretreatment is essential to elucidating reaction steps involving the diluent surface. To test if the lack of its chemical affinity toward CO_2 was the reason, TG chemisorption experiments were performed at 375 °C using 15% CO_2−Ar. Results shown in Figure 9 indicate that both ethanol-treated and untreated Al_2O_3 demonstrated essentially the same CO_2 chemisorption kinetics and equilibrium capacity as the ZnO (Strem); the ZnO (Grillo) sample showed no measurable CO_2 chemisorption. This implies that the amount of CO_2 chemisorbed on a diluent surface is not affecting the Zn oxidation performance.

dx.doi.org/10.1021/cm503064f | Chem. Mater. 2014, 26, 6486−6495

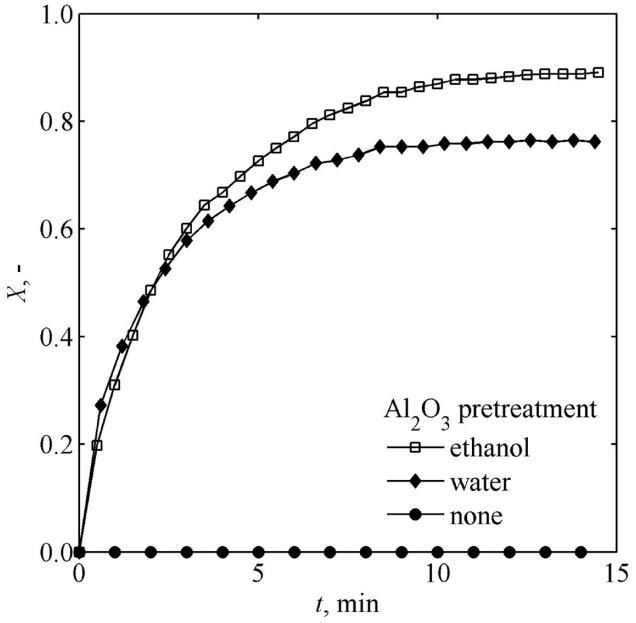

Figure 8. Effect of Al_2O_3 pretreatment on conversion of Zn during reaction of 50 wt % Zn–Al_2O_3 blends at 375 °C in 15% CO_2–Ar.

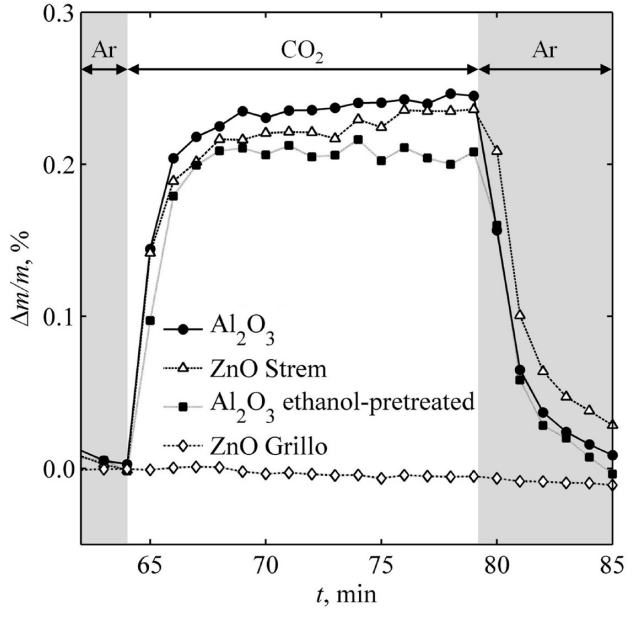

Figure 9. Relative mass change during TG chemisorption of CO_2 from 15% CO_2–Ar on ZnO (Strem), ZnO (Grillo), ethanol-treated Al_2O_3, and untreated Al_2O_3 materials at 375 °C.

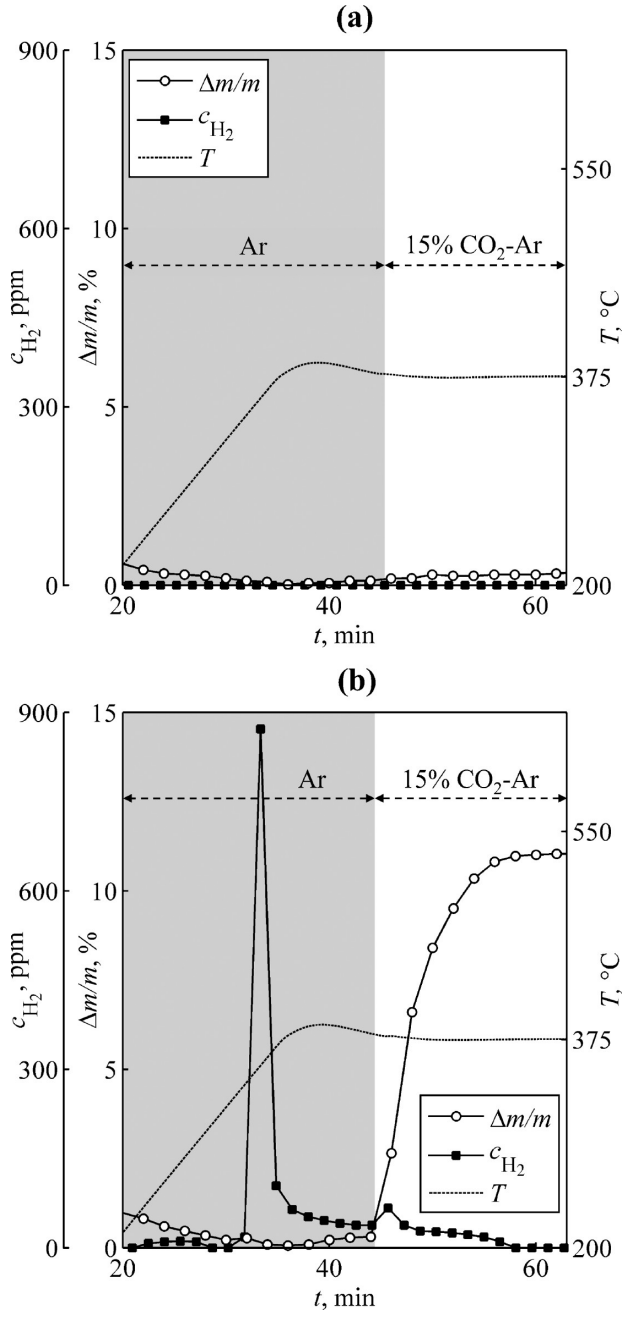

Figure 10. Temporal H_2 concentration in effluent gas (filled symbols), sample mass (open symbols), and temperature (dashed line) during temperature-programmed TG heat-up in Ar (shaded area) followed by oxidation in 15% CO_2–Ar of 50 wt % Zn–Al_2O_3 blends prepared with (a) untreated and (b) ethanol-pretreated Al_2O_3.

A clue to the reaction mechanism responsible for enhanced oxidation in the presence of pretreated Al_2O_3 is revealed by the temporal H_2 concentrations in the effluent gas acquired during preheating of the sample to the reaction temperature in Ar. Figure 10 compares these alongside relative sample masses and temperatures for two TG runs performed with blends containing either untreated (Figure 10a) or ethanol-pretreated Al_2O_3 as diluent (Figure 10b). Both blends were subjected to the identical standard experimental schedule. In the case of ethanol-pretreated Al_2O_3, a significant H_2 peak is observed during the initial heating in Ar and the reaction begins immediately upon exposure to CO_2. In contrast, in the presence of untreated Al_2O_3 no H_2 evolution is observed during preheating and the reaction does not proceed upon exposure to CO_2. The later H_2 peak observed during the onset of the reaction with CO_2 are attributed to trace H_2O impurities in the Zn material used[26] as they are common for all experiments regardless of whether or which diluent was used.

H_2 evolution was not observed during preheating blends of untreated Al_2O_3 with ethanol-pretreated Zn (not shown). Namely, high Zn conversion after subsequent exposure to CO_2 was found to be related solely to the modifications of the Al_2O_3 surface induced by the ethanol pretreatment. Moreover, a 50 min thermal treatment of ethanol-pretreated Al_2O_3 at 375 °C under Ar purge reversed the effect of the pretreatment; the Zn

dx.doi.org/10.1021/cm503064f | Chem. Mater. 2014, 26, 6486–6495

subsequently blended with the equal mass of this thermally treated ethanol-washed Al_2O_3 showed no reactivity with CO_2.

The above findings imply that the H_2 evolution from pretreated samples during preheating could be related to the oxidation of Zn on the ethanol pretreated Al_2O_3 surface. A plausible explanation is that ethanol pretreatment hydroxylates the Al_2O_3 surface. The surface hydroxyl groups then react with Zn(g) sublimated from the Zn particles at elevated temperatures producing H_2 and ZnO:

$$Zn(g) + 2AlO(OH)(s) \rightarrow Al_2O_3(s) + ZnO(s) + H_2(g) \quad (5)$$

This reaction has also been used to explain the facilitating effect of hydroxylated Al_2O_3 on deposition of various other metals from the vapor phase.[27−29] Once the ZnO seeds are formed on the Al_2O_3 surface, they facilitate the subsequent reaction of Zn with CO_2 in the same way the ZnO diluent particles in Zn-ZnO blends do. It is believed that the activation of Al_2O_3 by the water pretreatment demonstrated in Figure 8 is caused by the very same effect. If, however, hydroxylated Al_2O_3 is heated to 375 °C in the absence of Zn(g), the hydroxyl groups are desorbed. Therefore, the formation of the ZnO seeds during subsequent heating up in the presence of Zn(g) is precluded.

The effect of the ZnO surface area on the Zn conversion and the sensitivity of the reaction on the diluent surface chemistry both imply the growth of ZnO on the diluent surface as a reaction path parallel to the formation of the impervious ZnO scale over the surface of the Zn particles. In order to provide conclusive evidence for this reaction path, a sample of Zn blended with equal weight of ethanol-treated Al_2O_3 was reacted for 3 min in 15% CO_2−Ar at 375 °C to conversion of $X \sim 0.5$. The reaction product is then cooled in Ar to room temperature and analyzed by SEM, TEM, and STEM-EDX. As the same reaction mechanism is assumed to govern the oxidation of both Zn-ZnO (i.e., solar Zn) and Zn-(ethanol-treated Al_2O_3) blends, the ethanol-treated Al_2O_3 was chosen as diluent from two reasons: (a) it is chemically distinguishable from the reaction product (ZnO) in EDX and (b) because of a small size and polyhedral shape of its particles it can be visually differentiated from the larger and round Zn particles in SEM and TEM.

The SEM image enclosed as Figure 11 reveals two types of particles in the postreaction product: the spherical, hollow, ruptured scales that are reminiscent of the original Zn particles and agglomerates of smaller polyhedral particles resembling the Al_2O_3 material shown in Figure 2e,f. The scales are believed to represent ZnO; their appearance is substantially different from the thick, homogeneous, nonruptured scales completely covering the Zn particles that were observed by Loutzenhiser et al.[8] after reaction of undiluted Zn at 400 °C in 15% CO_2−Ar. As the sample represented by Figure 12 reacted only partially ($X \sim 0.5$), a certain amount of reactive Zn was expected to still remain within the scales.

The region of the sample outlined by the white square in Figure 12 was further analyzed with STEM-EDX. This particular particle agglomerate was targeted for these analyses because it resembled the alumina particles (Figure 2e,f). Moreover, it was reasonably isolated from the surrounding particles resembling the original Zn particles that were thus likely to contain both the Zn and ZnO phases. The latter was of a particular interest as the detection of spurious X-rays generated outside the investigated area due to electron scattering or X-ray fluorescence has been a known shortcoming of EDX analysis.[30]

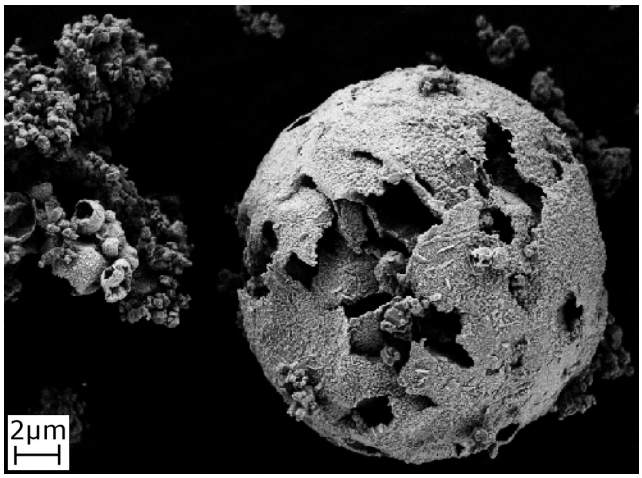

Figure 11. SEM image of a 50 wt % Zn-(ethanol-treated Al_2O_3) blend converted to $X \sim 0.5$ in 15% CO_2−Ar at 375 °C.

The acquired high resolution TEM images of several Al_2O_3 particle agglomerates did not reveal the presence of the distinctive ZnO and Al_2O_3 phases. Although they did indicate some variability in the contrast across the investigated region (Figure S3 in the Supporting Information), this variability was rather gradual thus implying the spatial distribution of the sample thickness rather than the differences in the atomic numbers.[30] On the other hand, the STEM-EDX analysis (Figure 12, right) did reveal peaks of O, Al, and Zn together with those of C and Cu. The latter two peaks are the artifacts caused by the sample-supporting film and the Cu-grid over which the sample was suspended. The strong Al peak confirmed that the visual resemblance to an Al_2O_3 agglomerate had merit in choosing the sample region to be analyzed. The O peak was thus at least partly caused by the Al_2O_3 agglomerate. Whether it also reflected the ZnO deposited over the Al_2O_3 surface depended merely on ruling out that the Zn peak originated from spurious reflections by the Zn and/or ZnO phases located outside the scanned region. The latter was achieved by comparing the intensities of the Cu and Zn peaks while considering that substantially more Cu than Zn was present by mass in the surroundings of the scanned sample region. As the Cu−Zn Cliff-Lorimer factor is of the order of 1,[30] if the analysis were falsified by spurious radiation from the surrounding Zn particles the intensity of the Zn peak would not be as strong compared to the intensity of the Cu peak. Therefore, it has been concluded that the acquired Zn peak reflected the presence of the ZnO layer uniformly distributed over the Al_2O_3 diluent surface by the growth from the seed ZnO sites formed per eq 5.

3.5. Mechanism of Oxidation of Zn Diluted with ZnO.

The experimental findings and the analytical evidence presented in the previous sections provide a basis for refining the mechanism of Zn oxidation by H_2O and CO_2 in the presence of ZnO stipulated by Stamatiou et al.[22] Namely, a gas-phase reaction of Zn(g) with either of the oxidants producing ZnO nanoclusters is ruled out as a pertinent reaction path because it would lead to high conversions irrespective of the diluent employed in the experiments. Instead, as illustrated by Figure 13a for the case of CO_2 as oxidant, the ZnO product is formed by parallel reactions around the Zn particles (solid

dx.doi.org/10.1021/cm503064f | Chem. Mater. 2014, 26, 6486−6495

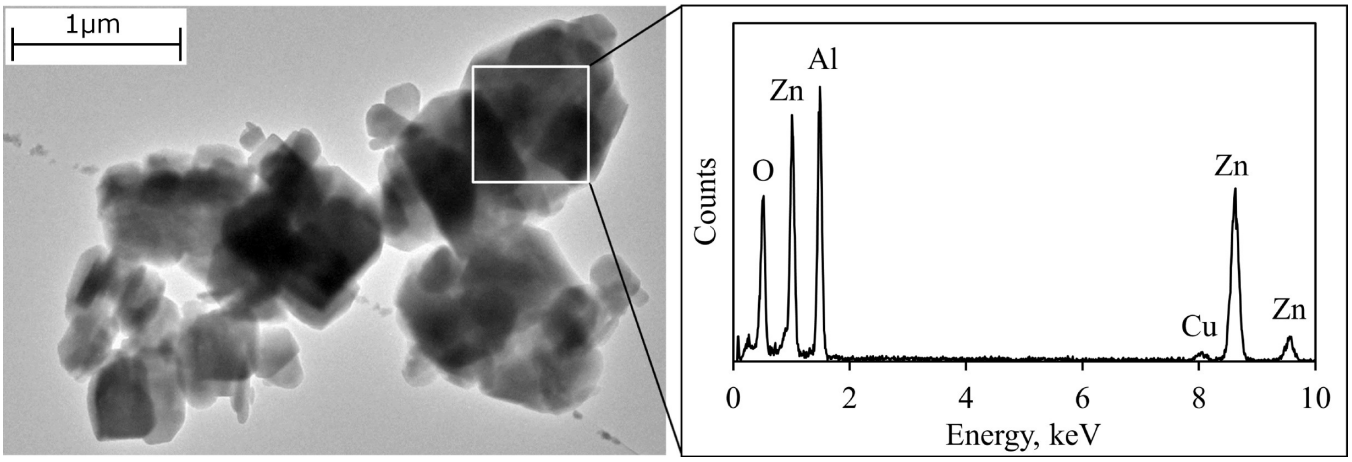

Figure 12. TEM image of an Al_2O_3 agglomerate from a 50 wt % Zn-(ethanol-treated Al_2O_3) blend reacted to $X \sim 0.5$ (left) and the results of the EDX elemental analysis over the segment outlined by the white square (right).

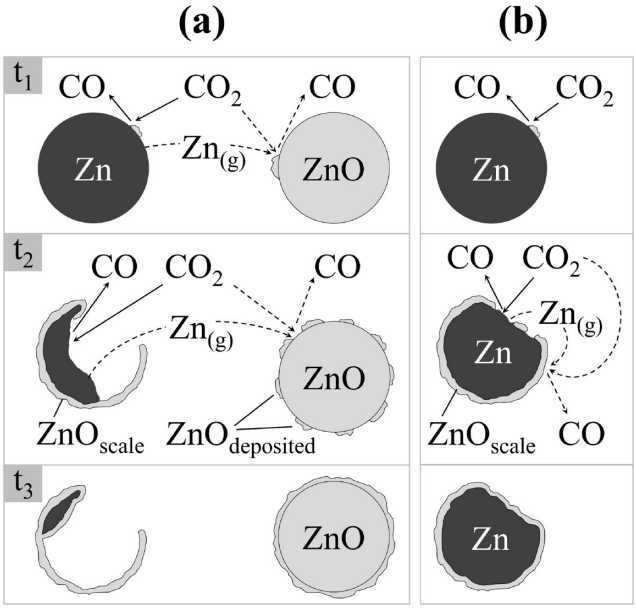

Figure 13. Schematic of the mechanism proposed for the oxidation of metallic Zn with CO_2 in the presence (a) and the absence (b) of ZnO diluent. A similar reaction mechanism is expected for the oxidation with H_2O.

lines) and on the ZnO seed sites at the surface of the diluent particles (dashed lines). In the early stage of the reaction (t_1), a thin ZnO scale quickly develops over the surface of the Zn particles leaving apertures and crevices for the passage of the sublimated Zn(g) toward the ZnO diluent and oxidants toward the reminder of the Zn particles ($t_2 > t_1$). The lateral scale growth eventually blocks the Zn surface, thereby inhibiting further Zn sublimation ($t_3 > t_2$). In the absence of a ZnO diluent (Figure 13b), the Zn sublimation is substantially slower, thus less Zn escapes through the apertures before they close. The enclosed Zn may further react only via a rather slow solid-state diffusion through the ZnO scale.[31] Therefore, the proposed mechanism stipulates that the maximum conversion of Zn is governed by the ratio of the ZnO scale growth and the Zn sublimation rates and that the presence of a ZnO diluent facilitates the latter.

For a given temperature, pressure, and coverage of the Zn surface, the only remaining parameter controlling the Zn sublimation rate is the difference between the equilibrium vapor pressure of Zn at the Zn surface and the vapor pressure of Zn in the surrounding gas. In spite of low equilibrium Zn vapor pressures for the investigated temperature range, it has been shown that the sublimation rate of Zn can be rather fast in high vacuum (~30 s for a ~2 μm particle).[32] Therefore, the Zn sublimation may be sustained by an effective sink of Zn(g) outside the Zn particles that is provided by a fast reaction at the ZnO sites on the diluent particles. Although the information available at present is not sufficient to discriminate among potential surface reactions involving adsorbed Zn and/or oxidants, the following scenarios are consistent with both experimental findings of this work and the literature.

3.5.1. Metallic Zn Deposited on the ZnO Sites from Sublimated Zn(g) and Then Oxidized by the Fast Reaction with Either H_2O or CO_2. The observed difference in the effects of ZnO (facilitating) and Al_2O_3 (no effect) as diluents in the Zn oxidation with CO_2 may be supported by the difference in the interaction of Zn(g) with ZnO and Al_2O_3 surfaces. The crystal structure of the ZnO surface inherently provides sites for Zn(g) deposition. Furthermore, ZnO shows nonstoichiometric behavior permitting the presence of excess Zn in the crystal which may facilitate incorporation of metallic Zn from Zn(g) on its surface.[33] On the other hand, it has been reported that Zn(g) does not interact with Al_2O_3 at temperatures within the investigated range.[34]

3.5.2. Diluent Surface Activates Oxidants for a Fast Reaction with Zn(g). Because an Al_2O_3 diluent does not facilitate the Zn oxidation with CO_2, this hypothesis implies that the CO_2 chemisorbs differently on the ZnO and Al_2O_3 surfaces, yielding the active oxygen on the ZnO only. On the other hand, H_2O may hydroxylate either of the diluents. The surface hydroxyls may then react with Zn(g) to provide the initial ZnO sites on the Al_2O_3. Once these sites are formed, they participate in the further Zn oxidation in the same way the ZnO diluent does.

4. SUMMARY AND CONCLUSIONS

This work investigates the mechanism of oxidation of metallic Zn in blends with ZnO or Al_2O_3 diluents prepared from well-characterized commercial powders. The effects of diluent surface area and ethanol- or water-pretreatment of the starting

dx.doi.org/10.1021/cm503064f | Chem. Mater. 2014, 26, 6486−6495

powders were explored within 350−400 °C by thermogravimetry using CO_2 or H_2O in mixtures with Ar as oxidants.

The presence of a ZnO diluent facilitates oxidation by either CO_2 or H_2O. Because of substantial sintering of samples, the repeatability of experiments performed in 8−30% H_2O−Ar was poor. Unless pretreated with ethanol or water, Al_2O_3 facilitates oxidation by H_2O only. The participation of the pretreated Al_2O_3 in the oxidation by CO_2 has been attributed to the formation of the ZnO seed sites on its surface. It is believed that these sites were formed in situ during heat-up to the reaction temperature in Ar by the reaction of Zn vapor with hydroxilated Al_2O_3 surface. Electron microscopy and EDX spectroscopy have supported this hypothesis by revealing substantial deposition of produced ZnO on the surface of pretreated Al_2O_3.

The refined Zn oxidation mechanism stipulates that the maximum achievable conversion of Zn is governed by the ratio of the ZnO scale growth over the Zn surface and the Zn sublimation rates. The presence of a ZnO diluent facilitates the latter by serving as an effective sink for Zn(g), thereby increasing the driving force for the diffusion of sublimated Zn from the surface of the solid Zn. It is not clear whether the ZnO surface provides the sink for Zn(g) by its affinity for Zn atoms or by its interaction with oxidants that activates them for a fast reaction with Zn(g).

■ ASSOCIATED CONTENT

Supporting Information

High-resolution TEM image, SEM images, and temporal conversion data. This material is available free of charge via the Internet at http://pubs.acs.org.

■ AUTHOR INFORMATION

Corresponding Author

*E-mail: zjovanovic@ethz.ch.

Notes

The authors declare no competing financial interest.

■ ACKNOWLEDGMENTS

We gratefully acknowledge the financial support by the Swiss Federal Office of Energy (Contract SI/500660-01) and by European Research Council under the European Union's ERC Advanced Grant (SUNFUELS, Grant No. 320541). The authors thank Dr. Eszter Barthazy (Electron Microscopy Centre EMEZ, ETH-Zurich) for performing the TEM and EDX analyses and contributing to the interpretation of the results, Alwin Frei (Solar Technology Laboratory, Paul Scherrer Institute) for providing the SEM images, and Dr. Jonathan Scheffe for fruitful discussions of the manuscript.

■ NOMENCLATURE

c	concentration, mol/m^3
d	particle diameter, μm
$\overline{d}$	volume-based mean particle diameter, μm
$\Delta h°$	standard enthalpy of reaction, kJ/mol
M	molar mass, g/mol
m	sample mass, mg
m_0	sample mass before oxidation, mg
m_f	sample mass after complete oxidation, mg
Δm	mass change, mg
T	temperature, °C
t	time, min
w	mass fraction, −
X	conversion of Zn to ZnO, −

Abbreviations

EDX	energy-dispersive X-ray spectroscopy
GC	gas chromatographer
SEM	scanning electron microscopy
SSA	specific surface area
STEM	scanning transmission electron microscopy
TEM	transmission electron microscopy
TG	thermogravimetry

■ REFERENCES

(1) Steinfeld, A. *Int. J. Hydrogen Energy* **2002**, *27* (6), 611−619.
(2) Loutzenhiser, P. G.; Meier, A.; Steinfeld, A. *Materials* **2010**, *3* (11), 4922−4938.
(3) Villasmil, W.; Brkic, M.; Wuillemin, D.; Meier, A.; Steinfeld, A. *J. Sol. Energy Eng.* **2013**, *136* (1), 011016−011016.
(4) Steinfeld, A.; Kuhn, P.; Reller, A.; Palumbo, R.; Murray, J.; Tamaura, Y. *Int. J. Hydrogen Energy* **1998**, *23* (9), 767−774.
(5) Venstrom, L. J.; Davidson, J. H. *J. Sol. Energy Eng.* **2011**, *133* (1), 011017.
(6) Gstoehl, D.; Brambilla, A.; Schunk, L.; Steinfeld, A. *J. Mater. Sci.* **2008**, *43* (14), 4729−4736.
(7) Schunk, L. O.; Haeberling, P.; Wepf, S.; Wuillemin, D.; Meier, A.; Steinfeld, A. *J. Sol. Energy Eng.* **2008**, *130*, 021009.
(8) Loutzenhiser, P.; Gálvez, M.; Hischier, I.; Stamatiou, A.; Frei, A.; Steinfeld, A. *Energy Fuels* **2009**, *23* (5), 2832−2839.
(9) Loutzenhiser, P. G.; Barthel, F.; Stamatiou, A.; Steinfeld, A. *AIChE J.* **2011**, *57* (9), 2529−2534.
(10) Bazán, J. C.; Gschaider, M. E.; Alimenti, G. A. *J. Therm. Anal. Calorim.* **1999**, *55* (2), 569−579.
(11) Weidenkaff, A.; Reller, A. W.; Wokaun, A.; Steinfeld, A. *Thermochim. Acta* **2000**, *359* (1), 69−75.
(12) Ernst, F. O.; Steinfeld, A.; Pratsinis, S. E. *Int. J. Hydrogen Energy* **2009**, *34* (3), 1166−1175.
(13) Nakamura, R.; Lee, J. G.; Tokozakura, D.; Mori, H.; Nakajima, H. *Mater. Lett.* **2007**, *61* (4), 1060−1063.
(14) Berman, A.; Epstein, M. *Int. J. Hydrogen Energy* **2000**, *25* (10), 957−967.
(15) Ernst, F. O.; Tricoli, A.; Pratsinis, S. E.; Steinfeld, A. *AIChE J.* **2006**, *52* (9), 3297−3303.
(16) Wegner, K.; Ly, H. C.; Weiss, R. J.; Pratsinis, S. E.; Steinfeld, A. *Int. J. Hydrogen Energy* **2006**, *31* (1), 55−61.
(17) Melchior, T.; Piatkowski, N.; Steinfeld, A. *Chem. Eng. J.* **2009**, *64* (5), 1095−1101.
(18) Weiss, R. J.; Ly, H. C.; Wegner, K.; Pratsinis, S. E.; Steinfeld, A. *AIChE J.* **2005**, *51* (7), 1966−1970.
(19) Abu Hamed, T.; Davidson, J. H.; Stolzenburg, M. *J. Sol. Energy Eng.* **2008**, *130* (4), 041010−041010.
(20) Venstrom, L. J.; Davidson, J. H. *Chem. Eng. J.* **2013**, *93*, 163−172.
(21) Abanades, S. *Ind. Eng. Chem. Res.* **2012**, *51* (2), 741−750.
(22) Stamatiou, A.; Steinfeld, A.; Jovanovic, Z. R. *Ind. Eng. Chem. Res.* **2013**, *52* (5), 1859−1869.
(23) Stamatiou, A.; Loutzenhiser, P. G.; Steinfeld, A. *AIChE J.* **2012**, *58* (2), 625−631.
(24) Dollimore, D.; Spooner, P. *Trans. Faraday Soc.* **1971**, *67*, 2750−2759.
(25) Lv, M.; Zhou, J.; Yang, W.; Cen, K. *Int. J. Hydrogen Energy* **2010**, *35* (7), 2617−2621.
(26) Porter, F. C. *Zinc Handbook: Properties, Processing, and Use in Design*; Dekker: New York, 1991.
(27) Chambers, S. A.; Droubay, T.; Jennison, D. R.; Mattsson, T. R. *Science* **2002**, *297* (5582), 827−831.
(28) Jennison, D. R.; Mattsson, T. R. *Surf. Sci.* **2003**, *544* (2−3), L689−L696.

(29) Fujimori, Y.; Kaden, W. E.; Brown, M. A.; Roldan Cuenya, B.; Sterrer, M.; Freund, H.-J. *J. Phys. Chem. C* **2014**, *118* (31), 17717−17723.
(30) Williams, D. B.; Carter, C. B. *Transmission Electron Microscopy: A Textbook for Materials Science*; Springer: New York, 2009.
(31) Moore, W. J.; Lee, J. K. *Trans. Faraday Soc.* **1951**, *47* (0), 501−508.
(32) Tringe, J. W.; Levie, H. W.; El-Dasher, B. S.; Swift, R.; Wall, M. A. *Appl. Phys. Lett.* **2011**, *98* (24), -.
(33) Hirschwald, W.; Bonasewicz, L.; Grade, M.; Hofmann, D.; Krebs, S.; Littbarski, R.; Neumann, G.; Grunze, M.; Kolb, D.; Schulz, J. *Curr. Top. Mater. Sci.* **1981**, *7*, 143−482.
(34) Rodriguez, J. A.; Kuhn, M.; Hrbek, J. *J. Phys. Chem.* **1996**, *100* (46), 18240−18248.